TRANSIENT ANALYSIS OF A NOISE SUPPRESSION METHOD WITH AERATING TECHNIQUES IN CAPILLARY TUBES

Yu ZHANG[1], Yicai LIU[1,2,*], Shiyan LIU[1], Zan GONG[1], and Likang WU[1]

[1]School of Energy Science and Engineering, Central South University, Changsha 410083 China

[2]Hunan Province Engineering Technology Research Center of New type of multifunctional building materials for energy storage and sound absorption, Shaoyang 420021 China

[*] Corresponding author; E-mail: lyccsu@csu.edu.cn

Flow-induced noise is closely related to the flow characteristics through an adiabatic capillary tube and a transition pipe, most existing methods for suppressing flow-induced noise are passive. An aerating technique is proposed based on the pressure feedback in the transition pipe to actively suppress flow-induced noise. Three-dimensional simulations of flashing are presented by performing the Schnerr-Sauer cavitation model coupling with the Mixture model. For the turbulence model, the large eddy simulation approach is used. With the installation of aerating module, the pressure fluctuation in the transition pipe is weakened significantly, and the phenomenon of bubble collapse is suppressed. Numerical results illustrate that the transient pressure of the monitoring points downstream of the capillary outlet oscillates seriously due to the bubble bursting; the shedding process of the bubble group is observed according to the vapor-liquid interface in the transition pipe. In addition, the oscillations of monitored transient pressure are suppressed with the application of aerating module. Then the noise source can be partially reduced actively in essence. This paper is devoted to understanding the two-phase flow characteristics of refrigerants in a transition pipe and presents a practical method to suppress noise near the capillary outlet.

Key words*: Homogeneous assumption, Schnerr-Sauer cavitation model, two-phase flow, bubble number density, unsteady simulation*

1. Introduction

Capillary tubes play the role of decreasing the pressure and temperature of the refrigerant and regulating its flow rate in small-scale vapor compression refrigeration systems [1-3]. The balance of the flow rate between the capillary tube and the compressor affects the evaporation temperature of the system directly, resulting in variations in the cooling capacity, input power, and performance coefficient of the refrigeration system. The matching of refrigerant charge and capillary size with the refrigeration system greatly influences the system's performance. Improper matching will cause an unstable state during system operation, such as occasional sharp noise due to the unsteady two-phase flow [4] and unstable

operation of the evaporator [5], which then affects system performance [6-7]. The traditional method for capillary matching is to consult the compiled capillary selection chart and empirical formulas, which requires a large amount of experimental data and consumes time and labor. However, the results are very inaccurate and the available refrigerants are limited. Consequently, to reduce the experimental work, it is of great significance to analyze the flow characteristics of refrigerants in capillary tubes and establish a fast calculation model with a relatively simple form and reliable accuracy for engineering applications.

Previous studies focused on the effect of refrigerant type on the induced noise in the capillary tube, and also indicating the relationship between the noise and the flow patterns [8]. Tatsumi [9] confirmed the flow-induced noise level is proportional to the pressure pulsation level, which was caused by the expansion of the gas at the end of the capillary tube, resulting in sudden variations in the sectional area. Han et al. [10] and Kim et al. [11] pointed out that in addition to the flow-induced noise inside the throttling device, random noise usually appears in the evaporator inlet pipe. Tannert and Hesse [12] showed that the main factor for noise excitation was variation in the flow pattern through the capillary outlet. Xia et al. [13] significantly suppressed flow-induced noise at the outlet of a capillary and reduced the peak sound pressure level by improving the structure of the transition pipe. In the transition pipe, flow features are highly correlated with noise sound pressure levels.

Despite the simple structure of the capillary tube, the flow characteristics are quite complicated, including turbulence, phase transition, and non-equilibrium phenomena under typical operating conditions, due to the flashing process. It is difficult to accurately predict the mass flow rate and pressure drop of refrigerants through the capillary tubes, as a result of these factors. Numerical researches focus on the establishment of reasonable mathematical models, such as the homogeneous flow model [14-15], the separated flow model [16-18], and the drift flow model [19-20]. Generally, the homogeneous model has been widely used in simulations of adiabatic capillary tubes due to its simplicity. For small-diameter capillary tubes, the velocity slip effect between the two phases can usually be ignored [21]. For most of the simulation studies of adiabatic capillary tubes, a one-dimensional hypothesis was adopted, and the accuracy of the simulation performance depended on the empirical correlations. However, it is difficult for numerical methods with the one-dimensional hypothesis to describe the complex flow characteristics in capillary tubes, and the variations in refrigerant flow properties across the cross-section of the capillary tube cannot be ignored.

Thanks to the rapid development of computer technology, computational fluid dynamics (CFD) has become a reliable method that commonly used in cavitation research, to acquire a comprehensive understanding of the characteristics of cavitation. The cavitation models based on Navier-Stokes control equations have been rapidly developed, and existing cavitation models are divided into two categories [22]:the interface tracking mothod based on single phase model, and the multi-phase model with an embedded cavitation interface. For computational robustness and efficiency consideration, most of the research work on cavitation adopts the latter method, among which, the homogeneous cavitation model is an effective tool to study cavitation flow in CFD simulations [23-24]. The Singhal model [25], Schnerr-Sauer model [26] and Zwart model [27] are widely used and developed in the simulations for valve cavitation [28], cryogenic cavitation [29] and tip-leakage vortex cavitation [30].

In addition, the cavitation flow is combined with strong turbulence, and the turbulence calculation has a great influence on the simulation results. For transient cavitation flows, the commonly used turbulence models include the corrected RNG k-ε model, the corrected k-ω model [31], detached eddy simulation (DES) [32] and large eddy simulation (LES). In recent years, LES model has attracted more and more attention and is expected to predict the flow field with vorticity more accurately. Long et al. [33] adopted LES combined with Zwart cavitation model to conduct numerical research on unsteady turbulent cavitation flow of twisted hydrofoil. By comparing with the experimental data, it is verified that the numerical method can give a better prediction on the complex cavitation flow around twisted hydrofoil. Considering thermodynamic effects, Wang et al. [24] studied the hydrofoil cavitation with LES, and revealed the relationship between cavitation and vorticity.

Refrigerant flashing is caused by the frictional pressure drop in the capillary tubes, excessive pressure drop caused by throttling can easily lead to cavitation and bubble collapse. Due to the existence of jet, it is easier to generate discrete vortex cavitation in jet shear layer. However, little has been reported on the unsteady numerical analysis of the refrigerant flow characteristics in the capillary tube and transition pipe. In the present research, a practical method to suppress flow-induced noise at the capillary outlet is proposed, as a result of pressure distribution and flow-induced noise being closely related. A branch tube is mounted in the transition pipe to guide fluid to the capillary outlet, from the downstream side. In the frame of homogeneous assumption, based on the Mixture model and combined with the Schnerr-Sauer cavitation model, three-dimensional unsteady simulations are studied with the commercial software Ansys Fluent 2020R1 [34]. Emphasis is focused on the two-phase flow characteristics in the transition pipe, and numerical simulations confirm the feasibility of the aerating module from the perspective of reducing bubbles collapse behavior. The results of this study help researchers comprehend the complex theory of the phase transformation in a capillary tube and transition pipe and additionally, a practical approach will be provided to reduce flow-induced noise in refrigeration units.

2. Numerical Methods

2.1. Physical Model and Assumptions

A homogeneous assumption is used in the present study, which assumes local equilibrium on a short spatial scale and considers the mixture of two phases as a pseudofluid. The major phase is the liquid phase, and the second phase is the vapor phase. This model solves the conservation equations, a mass, momentum, and energy equation for the mixture, and a volume fraction equation for the secondary phase. Assumptions are adopted as follows: (1) Three-dimensional flow is considered, with no-slip adiabatic wall boundary conditions. (2) It is a viscous and incompressible Newtonian fluid for the refrigerant in the liquid region. (3) The saturated vapor pressure of the refrigerant is related to temperature. (4) In the two-phase flow region, there is no slip velocity between the liquid phase and vapor phase. (5) On the basis of the inlet mass flow rate and the relevant velocity, turbulent flow is considered.

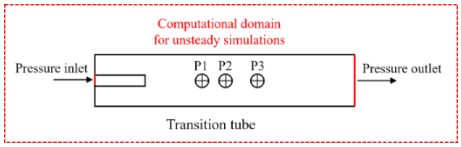

Figure 1. Schematic of the computational domain for unsteady simulations

For unsteady calculations, since the LES approach requires a high grid scale, especially the first layer height near the wall is quite small, which will greatly increase the computational cost. To save the calculation resource, only the transition pipe is selected as the calculation domain for unsteady simulations, as shown in Fig. 1. The inlet boundary conditions for the calculation domain in Fig. 1 are obtained from the quasi-steady state simulation results for the whole capillary tube. Three points are specified on the axis of the transition pipe, to monitor the transient static pressure, as shown in Fig. 1.

2.2. Mathematical Model

In this paper, the governing equations including the mass, momentum, energy conservation equations of the mixture phase, and the equation of the vapor phase volume fraction are solved.

2.2.1 Turbulence model

The LES model is adopted in transient simulations. Since the simulation results are greatly influenced by the choice of turbulence model, with the application of cavitation model. The LES model can simulate eddy flow well, and it has been paid enough attention in cavitation research [35]. Favre-spatial-filtering operations on the governing equations are required, and the filtered momentum equation is shown as follows:

$$\frac{\partial\left(\rho_m \bar{u}_i\right)}{\partial t}+\frac{\partial\left(\rho_m \bar{u}_i \bar{u}_j\right)}{\partial x_j}=-\frac{\partial \bar{p}}{\partial x_i}+\frac{\partial}{\partial x_j}\left(\mu_m \frac{\partial \bar{u}_i}{\partial x_j}\right)-\frac{\partial \tau_{ij}}{\partial x_j} \quad . \tag{1}$$

where the over-bars denote filtered quantities, and τ_{ij} is the sub-grid scale stress, it could be defined and calculated by eq. (2) and eq. (3):

$$\tau_{ij}=\rho_m\left(\overline{u_i u_j}-\bar{u}_i \bar{u}_j\right) \quad . \tag{2}$$

$$\tau_{ij}-\frac{1}{3}\tau_{kk}\delta_{ij}=-2\mu_t \bar{S}_{ij} \quad . \tag{3}$$

The subgrid-scale model is WALE (Wall Adapting Local Eddy-Viscosity), and the formula for μ_t and $\bar{S}_{ij}$ are shown in eq. (4) and eq. (5).

$$\mu_t=\rho L_S^2 \frac{\left(S_{ij}^d S_{ij}^d\right)^{3/2}}{\left(\bar{S}_{ij}\bar{S}_{ij}\right)^{5/2}+\left(S_{ij}^d S_{ij}^d\right)^{5/4}} \quad . \tag{4}$$

$$\bar{S}_{ij}=\frac{1}{2}\left(\frac{\partial \bar{u}_i}{\partial x_j}+\frac{\partial \bar{u}_j}{\partial x_i}\right) \quad . \tag{5}$$

2.2.2 Mass transfer model

The transport equation for vapor phase is presented in eq. (6), and eq. (7) can be used to describe the net mass transfer rate:

$$\frac{\partial}{\partial t}\left(\alpha\rho_v\right)+\nabla\cdot\left(\alpha\rho_v\boldsymbol{u}\right)=\dot{R}\ . \tag{6}$$

$$\dot{R}=\frac{\rho_v\rho_l}{\rho_m}\frac{d\alpha}{dt}\ . \tag{7}$$

According to the Schnerr-Sauer model [26], a definition formula for the vapor phase volume fraction α and bubble number density n_B is given by eq. (8):

$$\alpha=\frac{4}{3}n_B\pi R_B^3\Big/\left(1+\frac{4}{3}n_B\pi R_B^3\right)\ . \tag{8}$$

The surface tension term, second-order derivative term, and viscosity term are ignored, and vapor-liquid and liquid-vapor mass transfer rates could be determined in eq. (9) and eq. (10):

$$p>p_v,\ \dot{R}^-=3\frac{\rho_v\rho_l}{\rho_m}\alpha\left(1-\alpha\right)\left(\frac{\alpha}{1-\alpha}\frac{3}{4\pi}\frac{1}{n_B}\right)^{\frac{1}{3}}\sqrt{\frac{2}{3}\frac{p-p_v}{\rho_l}}\ . \tag{9}$$

$$p\le p_v,\ \dot{R}^+=3\frac{\rho_v\rho_l}{\rho_m}\alpha\left(1-\alpha\right)\left(\frac{\alpha}{1-\alpha}\frac{3}{4\pi}\frac{1}{n_B}\right)^{\frac{1}{3}}\sqrt{\frac{2}{3}\frac{p_v-p}{\rho_l}}\ . \tag{10}$$

Consequently, a proportional relationship exists between mass transfer rate and $\alpha\left(1-\alpha\right)$. Generally, the bubble radius is usually quite small (for example, 5×10^{-6} m in this paper). Rewrite $\alpha\left(1-\alpha\right)$ into the form as shown in eq. (11), as the n_B increases, the mass transfer rate increases as well.

$$\alpha\left(1-\alpha\right)=\frac{1}{\left(\frac{4}{3}n_B\pi R_B^3\right)^{-1}+2+\left(\frac{4}{3}n_B\pi R_B^3\right)} \tag{11}$$

Normally, the cavitation phenomenon inside the liquid is assumed to be isothermal. However, this assumption is no longer valid for simulating refrigerant flashing. According to Zhu et al.'s [29] and Zhang et al.'s [36] research, the thermal effect is considerable and must be considered for cryogenic liquid (including liquid N_2 and liquid H_2). Empirical calibration of the n_B in the Schnerr-Sauer model is essential to minimize the difference between the simulations and experimental data.

2.2.3 Boundary conditions and simulation approaches

Structured grids were adopted and performed by the software ICEM. To reduce the amount of calculation, a symmetric model is adopted, and local refinement near the tube wall is performed using a C-type grid, as shown in Fig. 2. To ensure the calculation accuracy, the mesh is locally refined near the jet boundary layer with a large velocity gradient due to the complex flow characteristics there. Five sets of mesh resolutions were designed to verify the solutions independence of the mesh for quasi-steady state simulations. The differences between the five sets of mesh are the value of the first layer height and a total number of grids. As Table 1 listed, the grid will have little effect on the mass flow rate, once the total cell number increase up to 1.18×10^6. For unsteady simulations, the Mesh 5 are adopted (total number of cells is 7.35×10^7), to meet the requirement of y^+ smaller than 5.

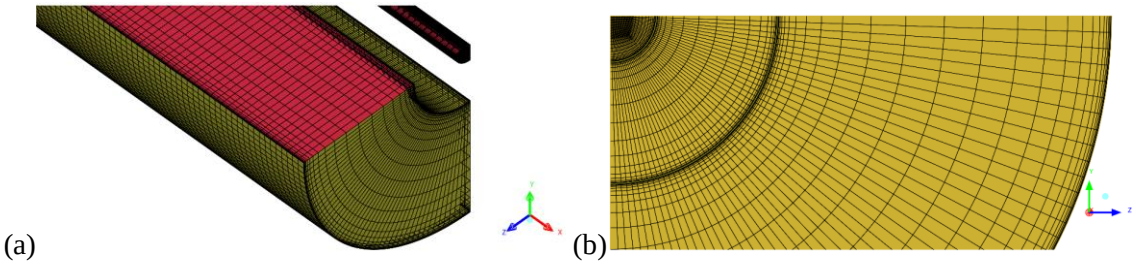

(a) (b)

Figure 2. Mesh distribution from the view isometric (a), and right (b)

Table 1. Results of the mesh-independence simulations

	The first layer height (m)	Total number of grids	Mass flow rate (kg/s)
Mesh 1	5.5×10^{-6}	3.1×10^{5}	8.77×10^{-5}
Mesh 2	3×10^{-6}	7.1×10^{5}	8.43×10^{-5}
Mesh 3	2.25×10^{-6}	1.18×10^{6}	8.36×10^{-5}
Mesh 4	2.1×10^{-6}	1.31×10^{6}	8.32×10^{-5}
Mesh 5	9×10^{-7}	7.35×10^{6}	8.35×10^{-5}

To ensure the accuracy of the LES simulations adopted in this paper, we checked the Q_c values of Mesh 5, according to the suggested criterions as proposed by Benard et al. The definition of Q_c is shown in Eqs. (12) and (13), and the value of Q_c is expected to be less than 0.2, as suggestd by Benard et al. [37] and proved to be effective in Ref.[33] .

$$\mathrm{Q_c} = \frac{E_{\mathrm{sgs}}}{E_{\mathrm{sgs}} + E_{\mathrm{R}}} \tag{12}$$

$$E_{\mathrm{sgs}} = C\left(\frac{\nu_{\mathrm{sgs}}}{\Delta}\right)^2 \tag{13}$$

where C = 100 is recommended. (The calculation results of Q_c with Mesh 5 are shown in Fig. 3, and the maximum Q_c occurs near the capillary outlet, and its value is about 0.194, which satisfies the requirement of below 0.2.

A pressure inlet boundary condition is adopted for the inlet of the computational domain, and a pressure outlet boundary condition is used at the outlet. The second-order upwind scheme is adopted for the momentum equation. Divergence methods for pressure and volume fraction are PRESTO! and QUICK, respectively. Coupled scheme is adopted for pressure-velocity coupling. The time step size is set to 1×10^{-5} s, less than the calculated reference values as suggested by Coutier-Delgosha et al. [38]. The thermodynamic and transport properties of the refrigerant are obtained from Refprop [39].

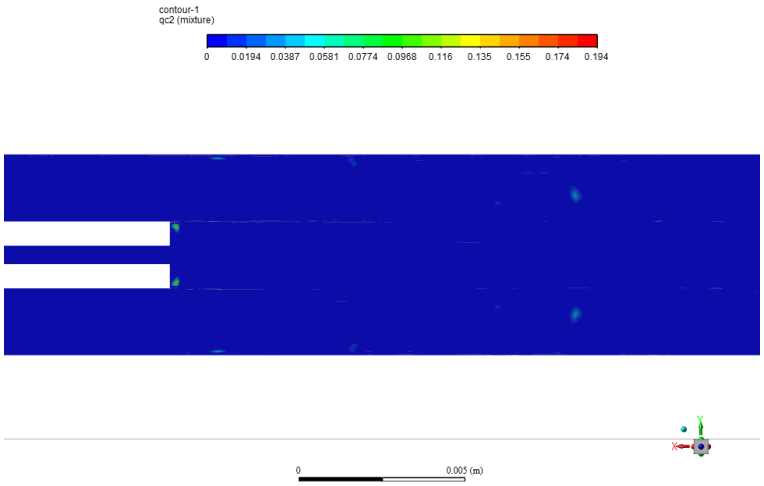

Figure 3. Distributions of Q_c on z=0 plane with Mesh 5

2.2.4 Model validation

Comparative analysis of the numerical results in the present model is conducted with numerical results in the literature [40], to verify the reliability of the present model. In this study, the n_B is modified and further determined for refrigerants by comparing the numerical results for pressure and temperature with experimental data in the literature. Simulations are carried out with different n_B values, and the results are shown in Fig. 3. As can be seen, once the n_B decreases to 10^7, the simulated values of pressure are consistent with those of Knabben et al.. The relationship between the n_B and the mass transfer rate is positive relativity, when the n_B is too high (for example, 10^9), the mass transfer source term is overestimated in the two-phase region, especially at the location near the flash point, resulting in the collapse of the pressure distribution curve in the two-phase region. Fig. 4(a) also illustrates the mass transfer rate along the axis of the capillary tube, as can be seen, in the two-phase region, there should generate a large amount of vapor phase. While the mass transfer rates are wrong estimated and even large negative values appear, when the value of n_B is too high.

In Fig. 4(b), the value of n_B is fixed at 10^7 in the simulations. As shown, there is little difference in the pressure profiles between the present model and Knabben et al.'s [40] numerical data. The flash points in Knabben et al.'s data are located at x_i=0.78 m and 0.67 m for 15 K and 10 K subcooling temperatures, respectively. In the present model, the flash points are located at 0.806 m and 0.715 m, and the relative deviations are approximately 3.3% and 6.7%, respectively. The above results show that for R600a, it is reasonable to choose the value of n_B at 10^7. This is slightly different with Zhu et al.'s [22] conclusions, that it is more accurate for cryogenic fluids including liquid N_2 and liquid H_2, that n_B equals 10^8.

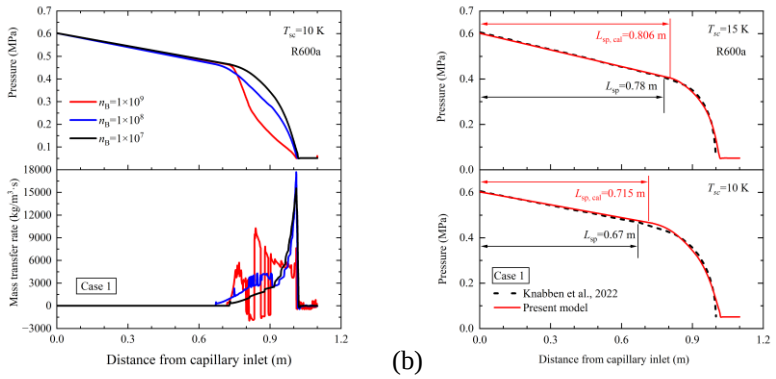

Figure 4. Simulated pressure profiles and flash points compared with the numerical data of Knabben et al. (2022) for R600a, (a) for various values of n_B; (b) n_B is fixed at 10^7

Consequently, in the Schnerr-Sauer cavitation model, n_B is suggested at 10^7 for R600a in this study. Moreover, the present model can be extended to a variety of refrigerants, by modifying n_B, in the case of comparison with experimental data.

3. Results and Discussions

3.1. Flow Characteristics

The working conditions are consistent with Knabben et al. [40], in the following simulations. Fig. 5 indicates the profiles of pressure, mass transfer rate, and velocity at the axis of the transition pipe. The pressure gradient is very high near the capillary outlet (x_i=1~1.015 m), and the flashing process still occurs in the capillary. Near the region of xi from 1.015 to 1.02 m, when the refrigerant sprays out from the capillary outlet, the flow section areas suddenly expand, and the pressure gradient increases distinctly because of partial flow resistance. However, due to the force of inertia of the fluid, a relatively high velocity is maintained for some distance. Then, the viscous force of the fluid gradually dominates, and the velocity decreases rapidly when subjected to shear forces. The kinetic energy is converted into potential energy, after which the pressure begins to recover. In the region of x_i from 1.02 to 1.05 m, at the initial stage of pressure recovery, the pressure gradient is about 6.84×10^5 Pa/m. However, as the pressure recovers, some of the bubbles collapse and condense back into the liquid phase. As the volume occupied by the bubbles fills with liquid phase, the pressure then drops slightly. When it drops below the saturated vapor pressure again, there will be a transfer from liquid phase to vapor-phase again. Generally, in this original model, the pressure downstream of the capillary outlet fluctuated and recovered gradually, and the corresponding mass transfer rate also oscillated. This indicated that the bubbles experience a complex process of growth, collapse, re-growth, and re-collapse the downstream of capillary outlet, accompanied by a large amount of energy loss and sharp noise radiation.

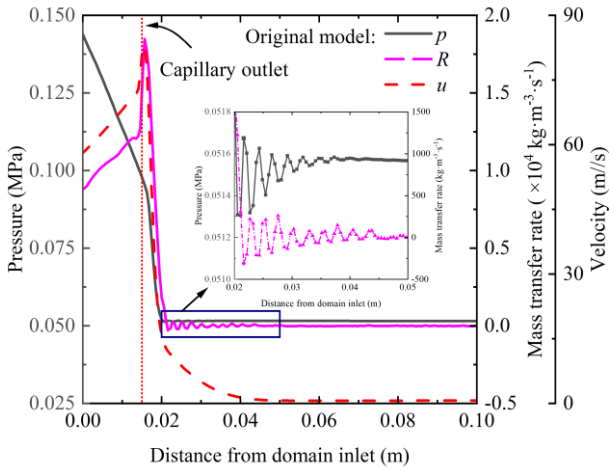

Figure 5. Distribution of flow characteristic parameters of R600a along the transition pipe

3.2. Unsteady State Flow Characteristics

Actually, the refrigerant flashing process inside a capillary tube is unsteady. When the RANS method is used to calculate the quasi-steady state process, the turbulent viscosity may be overpredicted by the $k-\varepsilon$ model and the development of eddy flow will be inhibited. Therefore, the bubble-shedding process in the phase transition region cannot be accurately simulated, and only the time-averaged values can be presented. Therefore, unsteady flow analysis is carried out in this study, by the LES approach. Three monitoring points were set downstream, about 10 mm (P1), 13 mm (P2), and 20 mm (P3) away from the capillary outlet, as Fig. 1 presented. Fig. 6 illustrates the variation of monitored transient pressure through flow time. As can be seen, the pressure oscillated periodically, and the oscillation amplitude at P2 is quite large, which may be caused by the bubble bursting. Fig. 7 shows the spectrum analysis of monitoring pressure after FFT transformation. 1×10^{-5} s is the sampling interval, and sampling time is 25 ms with 2500 sampling points. Consequently, the resolution of the FFT analysis is 40 Hz. The frequency of pressure oscillation in these three monitoring points is consistent, at about 193 Hz.

To analyze the unsteady shedding process of the bubble group in detail, the iso-surface of the vapor volume fraction at 12 flow time are illustrated in Fig. 8, and the time interval between every two images is 0.5 ms. The vapor volume fraction is set to 0.97, to demonstrate the interface between the vapor phase and liquid phase. As shown, the size of the vapor volume fraction iso-surface in one cycle increases first and then decreases, and the bubble group continuously formed from the inside of the mainstream zone and "flowed out" of the tail of the mainstream zone, and then gradually collapsed downstream. Time t1 is the beginning of a cycle, and during the flow time t1 to t6, the refrigerant bubble group is in the growth stage. From time t5, the bubbles at the leading edge begin to fall off and flow downstream with the main stream. Once the pressure gradually increase, the volume of these bubbles slowly shrink and these bubbles finally collapse. At t7-t11, the refrigerant bubble group begins to shrink. After t12, the growth and contraction process of the bubble group begins a next cycle.

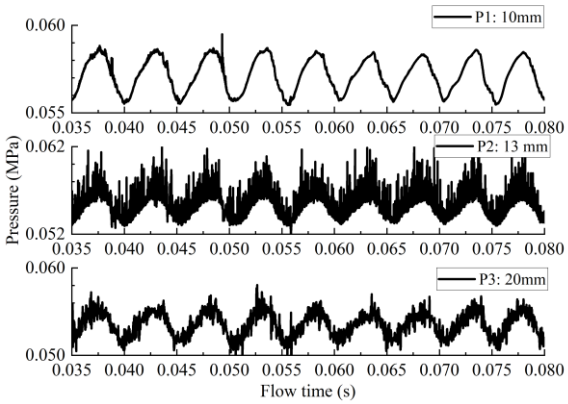

Figure 6. Transient pressure of the monitored three points in the transition pipe

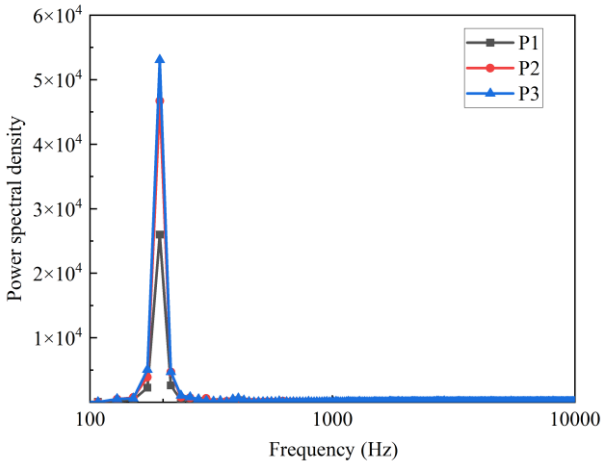

Figure 7. FFT analysis of the transient pressure

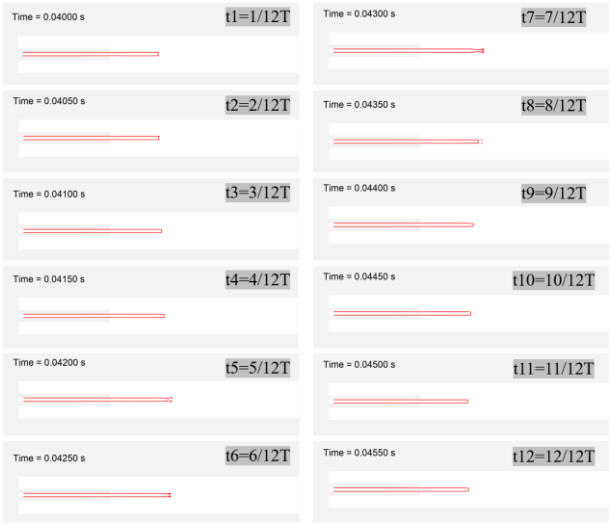

Figure 8. Iso-surface of vapor volume fraction equals 0.97

3.3. Aerating Techniques

A ‘negative pressure region’ occurs around the transition pipe wall near the capillary outlet, due to the high spraying velocity of the mainstream, which means that the static pressure downstream the transition pipe is slightly higher than that in the negative pressure region due to the vortex. Consequently, an aerating technique based on pressure feedback can be considered. If the bubble collapse phenomenon in the transition pipe is effectively reduced, then it will be benefit to suppress flow-induced noise near the capillary outlet (or the inlet of the evaporator). Recently, Zhang et al. [41] reported experimental results that confirmed the feasibility of applying aerating techniques to suppress flow-induced noise near the capillary outlet, and 2 dB decrease on average in the noise sound pressure level (SPL) was achieved. In this paper, numerical calculations are conducted to present the flow features in the transition pipe, which can provide a theoretical analysis of the working principle of the aerating techniques. Fig. 9 illustrates the schematic of the aerating module in the transition pipe, a branch tube is adopted to introduce refrigerant to the capillary outlet, from downstream side.

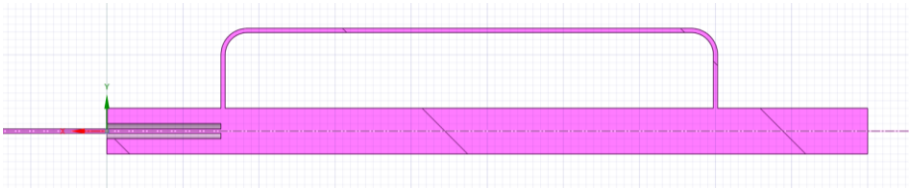

Figure 9. Schematic of the aerating model in a transition pipe

Fig. 10 presents two distribution curves of mass transfer rate and pressure along the transition pipe, for models with or without aerating techniques. After installing the aerating module, the pressure recovers more slowly, and the pressure gradient is about 3.63×10^{4} Pa/m at the initial stage of pressure recovery, which is about one order magnitude lower than that of without aerating techniques. And the pressure fluctuation phenomenon almost disappeared, therefore, the mass transfer rate fluctuates slightly around zero. This indicates that the phenomenon of bubble growth and collapse has been suppressed by aerating techniques.

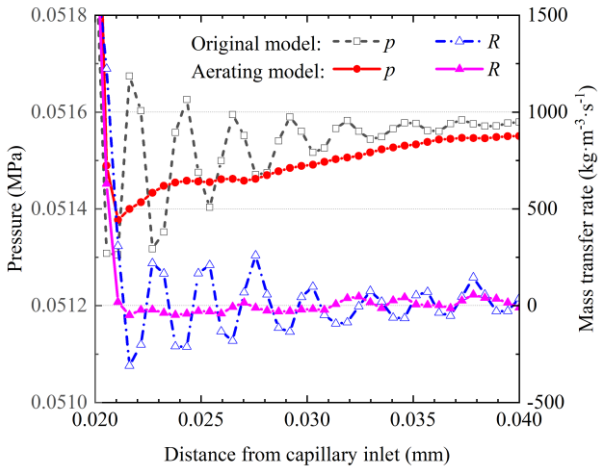

Figure 10. Distribution of pressure and mass transfer rate of R600a along the transition pipe

Similarly, the transient pressure are also be monitored and analyzed in unsteady simulations with aerating module, and the relative positions of these three monitoring points are consistent with that in Fig. 1. Results are shown in Fig. 11 and 12, as demonstrated, the transient pressure shows regular and periodic variation, while only slight oscillations are monitored. The amplitude of the pressure oscillation at the location of 13 mm downstream away from the outlet of the capillary, decreases from 5 kPa to almost zero after the application of aerating module. According to the research results from Tatsumi [9], the flow-induced noise level is proportional to the pressure pulsation level. Once the pressure oscillation magnitude has been suppressed, the flow-induced noise level will be suppressed accordingly. Besides, the FFT analysis indicates the frequency of pressure oscillation in these three monitoring points is about 170 Hz. This also indicates that the frequency of bubble group shedding decreases after adopting the aerating techniques, which is beneficial for suppressing the noise generated by bubble bursting.

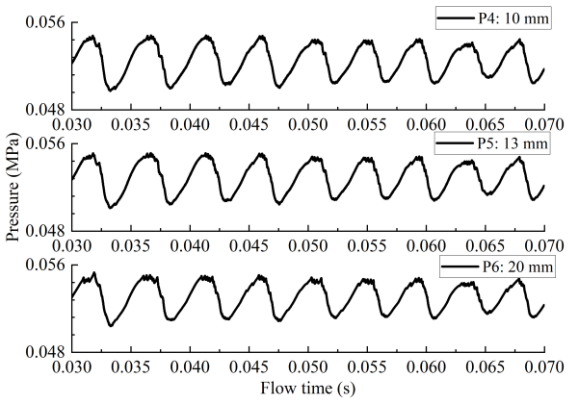

Figure 11. Transient pressure of the monitored three points in the transition pipe with aerating

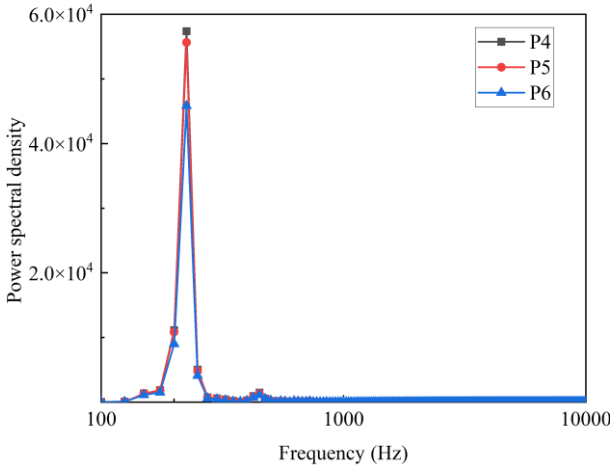

Figure 12. FFT analysis of the transient pressure with aerating

The bubble collapsing phenomena was effectively suppressed in a transition pipe, by installation an aerating module. In the future, CFD/CAE (computer-aided engineering) analysis will be carried out on the effects of aerating techniques on flow and sound characteristics in the transition pipe to analyze the

generation, propagation, and attenuation of two-phase flow-induced noise near the capillary outlet, providing a more theoretical basis for the noise suppression.

4. Conclusions

This paper presents an effective method to suppress flow-induced noise near the capillary outlet. The reliability of the calculation method is verified by comparing its results with the numerical data in the literature. The following conclusions have been put forward:

(1) The bubble number density (n_B) has a significant impact on flow characteristics during refrigerant flashing; $n_B=10^7$ is more accurate than other values for refrigerant R600a, according to the experimental results.

(2) The fluctuated pressure and bubble-collapsing phenomenon were suppressed in a transition pipe, when the aerating module has been installed.

(3) With the application of aerating module, the oscillations of transient pressure are suppressed and the frequency of bubble group shedding also decreases.

The refrigeration system will not be affected by the installation of aerating module (such as COP), and the aerating module is easy to be quick installed, which benefits to suppress the flow-induced noise, particularly in tranquil surroundings. Furthermore, unsteady flow and noise simulations will be carried out to reveal more transient flow characteristics in the capillary tubes and the transition pipes and illustrate the noise generation and suppression mechanism, in the future.

Acknowledgment

This research was funded by the National Natural Science Foundation of China (51776226), and supported by the Fundamental Research Funds for the Central Universities of Central South University (1053320214535).

Nomenclature

C - constant

E_R - resolved turbulent kinetic energy: $E_R = 1/2\left(\overline{u}_i'\overline{u}_i'\right)$ (m^2/s^2)

E_{sgs} - subgrid-scale turbulent kinetic energy (m^2/s^2)

L_S - mixing length for subgrid scales (m)

n_B - bubble number per unit volume of liquid

p - pressure (Pa)

p_v - vaporization pressure (Pa)

Q_c - a criterion to ensure enough explicit resolution of turbulent scales motions

$\dot{R}$ - net mass transfer rate

R_B - bubble radius (m)

S_{ij} - mean rate-of-strain tensor

t - time (s)

u - velocity (m/s)

Greek symbols

α - volume fractions of vapor

μ - dynamic viscosity (N·s/m^2)

μ_t - subgrid-scale turbulent viscosity (N·s/m^2)

ν_{sgs} - sub-grid kinematic viscosity (m^2/s)

ρ - density (kg/m^3)

τ - Reynolds stress (N)

τ_{ij} - sub-grid scale stress (N)

τ_{kk} - isotropic part of the subgrid-scale stresses (N)

Subscripts

l - liquid

m - mixture

t - turbulent

Symbols

Δ - local grid scale (m)

References

[1] Fatouh, M., Abou-Ziyan, H., Energy and exergy analysis of a household refrigerator using a ternary hydrocarbon mixture in tropical environment - Effects of refrigerant charge and capillary length, *Appl. Therm. Eng.*, *145* (2018), pp. 14-26.

[2] Sainath, K., *et al.*, Optimization of capillary tube dimensions using different Refrigerants for 1.5 ton mobile air conditioner, *Case Stud. Therm. Eng.*, *16* (2019), 100528.

[3] Bengtsson, P., Berghel, J., Study of using a capillary tube in a heat pump dishwasher with transient heating, *Int. J. Refrig.*, *67* (2016), pp. 1-9.

[4] Hartmann, D., Melo, C., Popping noise in household refrigerators: Fundamentals and practical solutions, *Appl. Therm. Eng.*, *1* (2013), pp. 40-47.

[5] Han, H.S., *et al.*, Reduction of the refrigerant-induced noise from the evaporator-inlet pipe in a refrigerator, *Int. J. Refrig.*, *33* (2010), pp. 1478-1488.

[6] Salem, T.K., *et al.*, Energy and exergy analysis study of heat exchanger in a refrigeration system with different lengths of capillary tube, *Int. J. Thermodyn.*, *23* (2020), 4, pp. 260-266.

[7] Tosun, T., Tosun, M., Heat exchanger optimization of a domestic refrigerator with separate cooling circuits, *Appl. Therm. Eng.*, *168* (2020), 114810.

[8] Filho, E.S., *et al.*, A State-of-the-art review on two-phase flow-pinduced noise in expansion Devices, *Heat Transfer Eng.*, *44* (2022), 1, pp. 1-23.

[9] Tatsumi, K., Study on noise caused by slug flow through a capillary tube, *Trans. JSME. B*, *63* (1997), 611, pp. 2392-2397.

[10] Han, H.S., *et al.*, Frequency characteristics of the noise of R600a refrigerant flowing in a pipe with intermittent flow pattern, *Int. J. Refrig.*, *34* (2011), 6, pp. 1497-1506.

[11] Kim, M.S., *et al.*, Development of noise pattern map for predicting refrigerant-induced noise in refrigerators, *J. Mech. Sci. Technol.*, *28* (2014), 9, pp. 3499-3510.

[12] Tannert, T., Hesse, U., Noise effects in capillary tubes caused by refrigerant flow. 16th International Refrigeration and Air Conditioning Conference, Purdue, 2016, pp. 1562-1572.

[13] Xia, Y.B., *et al.*, Experimental study on reducing the noise of horizontal household freezers, *Appl. Therm. Eng.*, *68* (2014), 1-2, pp. 107-114.

[14] Parmar, D., Atrey, M.D., Experimental and numerical investigation on the flow of mixed refrigerants through capillary tubes at cryogenic temperatures, *Appl. Therm. Eng.*, *175* (2020), 115339.

[15] Chingulpitak, S., Wongwises, S., A comparison of flow characteristics of refrigerants flowing through adiabatic straight and helical capillary tubes, *Int. Commun. Heat Mass Transfer*, *38* (2011), pp. 398-404.

[16] Furlong, T.W., Schmidt, D.P., A comparison of homogenous and separated flow assumptions for adiabatic capillary flow, *Appl. Therm. Eng.*, *48* (2012), pp. 186-193.

[17] García-Valladares, O., *et al.*, Numerical simulation of capillary tube expansion devices behaviour with pure and mixed refrigerants considering metastable region. Part I: mathematical formulation and numerical model, *Appl. Therm. Eng.*, *22* (2002), 2, pp. 173-182.

[18] García-Valladares, O., *et al.*, Numerical simulation of capillary-tube expansion devices behaviour with pure and mixed refrigerants considering metastable region. Part II: experimental validation and parametric studies, *Appl. Therm. Eng.*, *22* (2002), 4, pp. 379-391.

[19] Zareh, M., *et al.*, Numerical simulation and experimental analysis of refrigerants flow through adiabatic helical capillary tube, *Int. J. Refrig.*, *38* (2014), pp. 299-309.

[20] Zareh, M., *et al.*, Numerical simulation and experimental comparison of the R12, R22 and R134a flow inside straight and coiled helical capillary tubes, *J. Mech. Sci. Technol.*, *30* (2016), 3, pp. 1421-1430.

[21] Kim, L., *et al.*, An assessment of models for predicting refrigerant characteristics in adiabatic and non-adiabatic capillary tubes, *Heat Mass Transfer*, *47* (2010), 2, pp. 163-180.

[22] Zhu, J.K., *et al.*, Extension of the Schnerr-Sauer model for cryogenic cavitation, *European Journal of Mechanics B-Fluids*, 52 (2015), pp. 1-10.

[23] Wang, Z.Y., *et al.*,. Euler–Lagrange study of cavitating turbulent flow around a hydrofoil, *Phys. Fluids*, 33 (2021), 11, 112108.Sauer, J., Schnerr, G.H., Unsteady cavitating flow-A new cavitation model based on a modified front capturing method and bubble dynamics, In Proceedings of ASME Fluid Engineering Summer Conference, Boston, USA, 2000.

[24] Zwart, P.J., *et al.*, A Two-phase flow model for predicting cavitation dynamics, Proceedings of International Conference on Multiphase Flow, Yokohama, Japan, 2004.

[25] Valdés, J.R., *et al.*, Numerical simulation and experimental validation of the cavitating flow through a ball check valve, *Energ. Convers. Manage.*, *78* (2014), 1, pp. 776-786.

[26] Zhu, J.K., *et al.*, Interactions of vortices, thermal effects and cavitation in liquid hydrogen cavitating flows, *Int. J. Hydrogen Energy*, *41* (2016), pp. 614-631.

[27] Cheng, H.Y., *et al.*, A review of cavitation in tip-leakage flow and its control, *J. Hydrodyn.*, *33* (2020), 2, pp. 226-242.

[28] Zhang, D.S., *et al.*, Numerical prediction of cavitating flow around a hydrofoil using PANS and improved shear stress transport k-omega model, *Therm. Sci.*, *19* (2015), 4, pp. 1211-1216.

[29] Zhang, D.S., *et al.*, Detached eddy simulation of unsteady cavitation and pressure fluctuation around 3-D NACA66 hydrofoil. *Therm. Sci.*, *19* (2015), 4, pp. 1231-1234.

[30] Long, X.P., *et al.*, Large eddy simulation and Euler–Lagrangian coupling investigation of the transient cavitating turbulent flow around a twisted hydrofoil, *Int. J. Multiphas. Flow*, *100* (2018), pp. 41-56.

[31] Theory Guide, ANSYS, Fluent 2020R1 Documentation.

[32] Chen, H.Y., *et al.*, A new Euler-Lagrangian cavitation model for tip-vortex cavitation with the effect of non-condensable gas. *Int. J. Multiphas. Flow*, *134* (2021), 103441.

[33] Zhang, X.B., *et al.*, Calculation and verification of dynamical cavitation model for quasi-steady cavitating flow, *Int. J. Heat Mass Transfer*, *86* (2015), pp. 294-301.

[34] Benard, P., *et al.*, Mesh adaptation for large-eddy simulations in complex geometries, *Int. J. Numer. Methods Fluids*, 81 (2016), *12*, pp. 719-740.

[35] Coutier-Delgosha, O., *et al.*, Numerical simulation of the unsteady behaviour of cavitating flows, *Int. J. Numer. Meth. Fluids.*, *42* (2003), pp. 527–48.

[36] Lemmon, E.W., et al., REFPROP: Reference fluid thermodynamic and transport properties, NIST standard reference database, 23(8.0), 2007.

[37] Knabben, F.T., et al., A study of flow characteristics of electronic expansion valves for household refrigeration applications, *Int. J. Refrig.*, *113* (2020), pp. 1-9.

[38] Zhang, Y., *et al.*, Application of aerating techniques for noise suppression in capillary tubes, *AIP Adv.*, *12* (2022), 025324.

Received: 27.11.2022.
Revised: 06.04.2023.
Accepted: 11.04.2023.